Transverse energy propagation and interference of elliptical Gaussian beams

Jin Li[1,2,*], Shuang-cheng Tan[1]

[1]College of Physics, Chongqing University, Chongqing 401331, China

[2]Department of Physics and Chongqing Key Laboratory for Strongly Coupled Physics, Chongqing University, Chongqing 401331, China

*Corresponding author: cqujinli1983@cqu.edu.cn

Elliptical Gaussian beam (EGB) has many different physical properties from circular Gaussian beam. In this paper, the transverse energy flux and intensity of one and two coherent EGBs are studied. In our simulation, the transverse energy flux and intensity varying with waist ratio are discussed in detail. It has been found that through increasing the waist ratio, the transverse energy flux after interference would be strengthened significantly. Although the transverse energy flux is much weaker than the longitudinal energy flux, its signal to noise ratio has been verified to be strong enough for detection. Our derivations are still reasonable for another simulation with general experimental parameters. The simulation results are considered to be helpful for some physical experiments using the transverse energy flux of Gaussian beam, such as an important application in electromagnetic response produced by interaction of high-frequency gravitational waves.

Keywords: elliptical Gaussian beam, transverse energy flux, interference of EGBs.

1. Introduction

According to the fundamental laser model, the standard Gaussian beam (GB) is assumed with circular cross-section (*i.e.*, circular Gaussian beam (CGB)). However, in application, laser beams are often elliptical Gaussian beams (EGB, also called astigmatic Gaussian beam), such as in laser optics, material processing, and nonlinear optics [1]. The EGB can be generated by focusing a CGB with a cylindrical lens or refracting a CGB at obliquely incident angles [2]. In 1969, EGB was put forward by Arnaud and Kogelnik in theory [3], then it has been studied widely. Carter derived the expression for electromagnetic components of a EGB [4]. Duan and Lü studied the propagation properties of vectorial EGB beyond the paraxial approximation [5]. In experiment, the characteristics of the EGB propagation in various optical systems have been investigated extensively [1,6–12].

As one of the typical optical phenomena, interference of EGBs could lead to some meaningful effects on electro-magnetic field yielding the deviation of energy propagation from a single EGB, which are mainly manifested in the different changes of energy fluxes and intensities in the transverse directions given the waist ratio after interference. Furthermore, the extra-high frequency gravitational wave is possible to resonate with the electromagnetic resonance system designed by Lɪ *et al.* [13–19] and results in some distinguished signals on the transverse directions. And our previous works indicated the transverse energy of signal would be enhanced greatly using EGB with some appropriate waist ratios [20, 21]. Therefore, as an optic pilot study for extra-high frequency gravitational wave detection, here we pay attention to the transverse properties before and after the interference.

We have discussed transverse propagation characteristics and coherent effect of the CGBs [22]. In this work, the energy fluxes and intensities of a single EGB and interference between two coherent EGBs in transverse directions are derived and simulated with different waist ratios. Meanwhile the detectability of the transverse energy flux is also be discussed after considering some noises (*e.g.*, background photon flux, shot noise, noise from incomplete extinction).

2. The energy flux density and intensity

Intuitively, the cross-section of an elliptical Gaussian beam is elliptical rather than circular (*cf.* the energy flux on z axis in Fig. 1(a)). But as the standard Gaussian beam, an elliptical Gaussian beam can also provide a non-vanishing longitudinal electric and
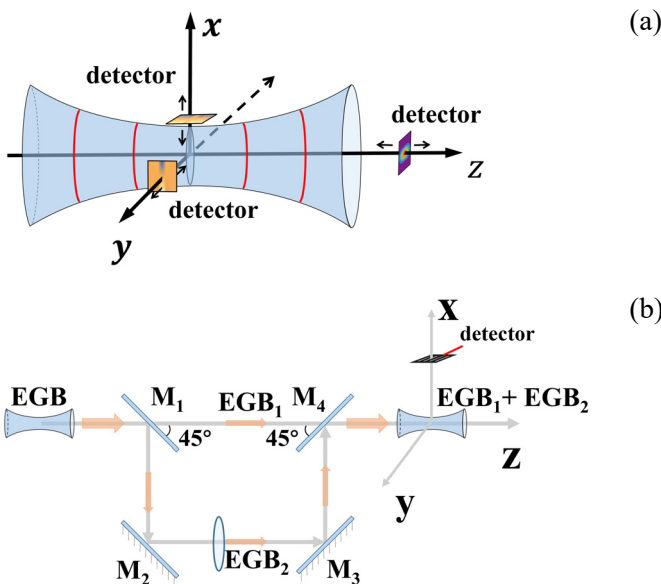

Fig. 1. (a) A single elliptical Gaussian beam and the energy propagation recorded by some photon detectors. (b) Optical path diagram for interference (directly cite Fig. 1(b) of [23]).

magnetic field components except on the waist plane. Therefore the detectors located in paraxial regions on x and y axes would record non-zero energy flux (*cf.* Fig. 1(a)). Generally, supposing the propagation direction on z-axis, one of the transverse electric components of an elliptical Gaussian beam (here choosing $\tilde{E}_x$) could be expressed as [23]

$$\tilde{E}_x = \psi = \exp\left(-\frac{x^2}{W_x^2} + \frac{ik}{2}\frac{x^2}{R_x}\right)\mathcal{F}(y, z) \tag{1a}$$

$$\mathcal{F}(y, z) = A\exp\left(-\frac{y^2}{W_y^2} + \frac{ik}{2}\frac{y^2}{R_y}\right)\left\{\left[(z/f_x)^2 + 1\right]^{1/2} + \left[(z/f_y)^2 + 1\right]^{1/2}\right\}^{-1/2}$$

$$\times \exp\left\{i\left[kz - \frac{\arctan(z/f_x) + \arctan(z/f_y)}{2} + \delta\right]\right\} \tag{1b}$$

where $k = 2\pi/\lambda$, $\omega = kc$ (c is the speed of light) is the angular frequency of GB, $f_x = \pi W_{0x}^2/\lambda$, $f_y = \pi W_{0y}^2/\lambda$, $W_x = W_{0x}[1 + (z/f_x)^2]^{1/2}$, $W_y = W_{0y}[1 + (z/f_y)^2]^{1/2}$ (W_{0x} and W_{0y} is the waist radius of GB on x and y axis, respectively), $R_x = z + f_x^2/z$, $R_y = z + f_y^2/z$ and δ is the initial phase of GB. $A = [4c\mu_0 P/\pi W_{0x}W_{0y}]^{1/2}$ is the amplitude of the Gaussian beam, where P is the power of laser and μ_0 is the permeability of vacuum. Then assuming $\tilde{E}_z = 0$, we can derive the other electric and magnetic field components according to the Maxwell equations in free space without charge and electric current, which are

$$\nabla \cdot \tilde{\mathbf{E}} = 0 \quad \Rightarrow \quad \tilde{E}_y = -\int \frac{\partial \tilde{E}_x}{\partial x}\,\mathrm{d}y = 2x\left(\frac{1}{w_x^2} - i\frac{k}{2R_x}\right)\int \tilde{E}_x\,\mathrm{d}y \tag{2}$$

$$\tilde{\mathbf{B}} = -i\nabla \times \tilde{\mathbf{E}}/\omega \quad \Rightarrow \quad \tilde{B}_x = \frac{i}{\omega}\frac{\partial \tilde{E}_y}{\partial z} \tag{3a}$$

$$\tilde{B}_y = -\frac{i}{\omega}\frac{\partial \tilde{E}_x}{\partial z} \tag{3b}$$

$$\tilde{B}_z = \frac{i}{\omega}\left(\frac{\partial \tilde{E}_x}{\partial y} - \frac{\partial \tilde{E}_y}{\partial x}\right) \tag{3c}$$

In order to acquire the information about the direction of energy propagation in the EM field, the Poynting vector is used to represent the energy flux density, which is the result of the vector product of the EM's electric and magnetic components as

$$\tilde{\mathbf{S}} = \frac{1}{\mu_0}\tilde{\mathbf{E}} \times \tilde{\mathbf{B}} \tag{4}$$

Considering the field pulsing with time quickly, the average value of the Poynting vector $\tilde{\mathbf{S}}$ over the time is $\overline{\tilde{\mathbf{S}}} = \langle \tilde{\mathbf{E}} \times \tilde{\mathbf{B}} \rangle / \mu_0$. The corresponding components are

$$\overline{\tilde{S}_x} = \frac{1}{2\mu_0} \operatorname{Re}(\tilde{E}_y^* \tilde{B}_z - \tilde{E}_z^* \tilde{B}_y) \tag{5a}$$

$$\overline{\tilde{S}_y} = \frac{1}{2\mu_0} \operatorname{Re}(\tilde{E}_z^* \tilde{B}_x - \tilde{E}_x^* \tilde{B}_z) \tag{5b}$$

where $\overline{\tilde{S}_x}$ and $\overline{\tilde{S}_y}$ indicate the averaged values of energy flux density on x- and y-axes, respectively, which generally can be recorded by charge-coupled device (CCD) at each point in space. In our simulation, the power of laser is chosen to be 1 mW, the wavelength $\lambda = 620$ nm, the initial phase is 1.32π. Once the optic paths are fixed, the phase difference between the light in branch 1 and 2 is constant, which will satisfy the interference requirement. The receiving surface is assumed as $\Delta s = (5 \times 5)$ mm, the detection distance $d = 1$ cm. For a single elliptical Gaussian beam, the $\overline{\tilde{S}_x}$, $\overline{\tilde{S}_y}$ and $\overline{\tilde{S}_z}$ are simulated numerically as Fig. 2. In the transverse paraxial regions, the energy fluxes also exist although they are very weak. Here the waist W_{0x} and W_{0y} are around 10^{-3}, yielding to the Rayleigh length $z_R \sim 100$ m. Therefore in the range of -0.02 m $< z < 0.02$ m, the changes of transverse flux density on the detection surface are around 10^{-10} W/m² as shown in Fig. 2.
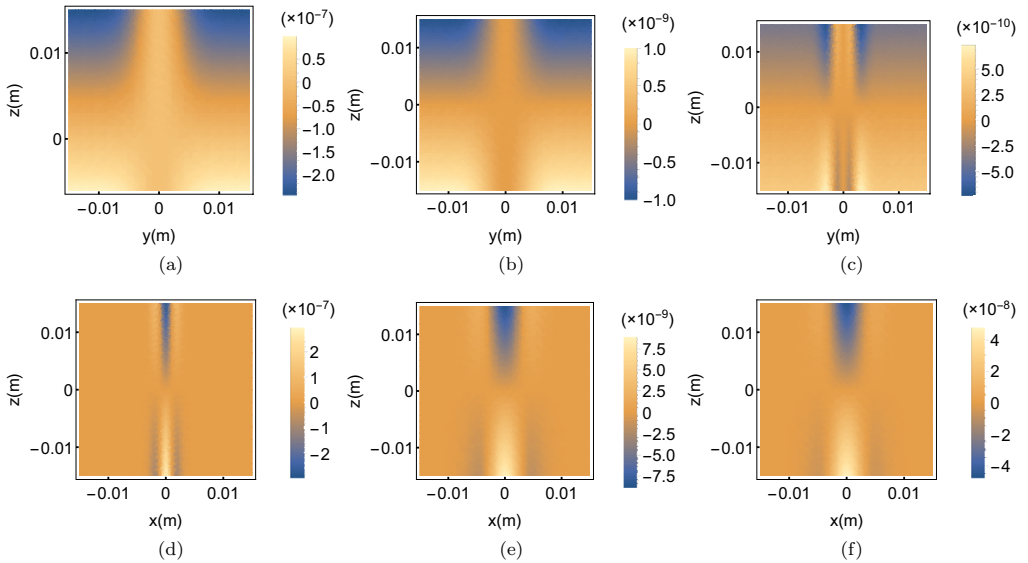

Fig. 2. The transverse energy flux density $\overline{\tilde{S}_x}$, $\overline{\tilde{S}_y}$ of a single beam with different beam waist ratios. The first column subplots (a) and (d) represent $\overline{\tilde{S}_x}$ and $\overline{\tilde{S}_y}$, respectively, with $W_{0x} = 0.002$ m and $W_{0y} = 0.005$ m; The second column subplots (b) and (e) represent $\overline{\tilde{S}_x}$ and $\overline{\tilde{S}_y}$, respectively, with $W_{0x} = W_{0y} = 0.005$ m; The third column subplots (c) and (f) represent $\overline{\tilde{S}_x}$ and $\overline{\tilde{S}_y}$, respectively, with $W_{0x} = W_{0y} = 0.002$ m.
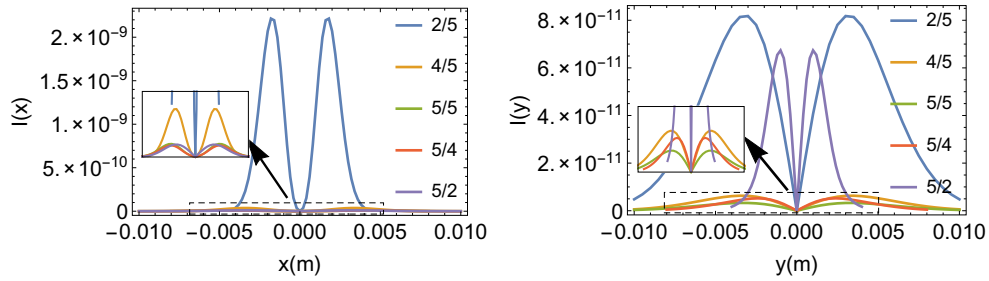
Fig. 3. The transverse intensity of a single beam with different waist ratios. The values on the legend represent the values of W_{0x}/W_{0y}. Here 2/5 represents $W_{0x} = 0.002$ m, $W_{0y} = 0.005$ m, while 5/2 represents $W_{0x} = 0.005$ m, $W_{0y} = 0.002$ m; 4/5 represents $W_{0x} = 0.004$ m, $W_{0y} = 0.005$ m, while 5/4 represents $W_{0x} = 0.005$ m, $W_{0y} = 0.004$ m; 5/5 represents $W_{0x} = W_{0y} = 0.005$ m.

If using photomultiplier tube (PMT) to detect the transverse intensities $I(x)$, $I(y)$, we also can find the features on transverse directions varying with waist ratios. Simulating the detector located at different positions (*cf.* Fig. 1(a)), given a receiving surface Δs of the detector, the corresponding intensities are

$$I(x) \;=\; \iint_{\Delta s} \overline{\tilde{S}}_x(x, y, z)\, \mathrm{d}y\, \mathrm{d}z \tag{6}$$

$$I(y) \;=\; \iint_{\Delta s} \overline{\tilde{S}}_y(x, y, z)\, \mathrm{d}x\, \mathrm{d}z \tag{7}$$

Figure 3 shows the $I(x)$, $I(y)$ varying with x, y. It can be found that the intensities along x and y axes have even symmetrical distributions and both vanish at the transverse center. With the increase of W_{0x}/W_{0y}, $I(x)$ decreases, but $I(y)$ increases with larger eccentricity of spot. Those are because

$$\overline{\tilde{S}}_x \;\sim\; \frac{A^2}{W_{0x}^4}, \qquad \overline{\tilde{S}}_y \;\sim\; A^2 \tag{8}$$

here $A \sim (W_{0x} W_{0y})^{-1/2}$ increases with eccentricity of spot. That means that the transverse intensity can be enhanced by appropriately changing the waist ratio with the fixed total power of laser.

3. Interference effect on the energy flux density and power

As a fundamental physical phenomenon of light propagation, interference occurs from the combination of two or more electromagnetic waveforms. As the simplest case, here we consider the interference from two elliptical Gaussian beams propagating on the same direction simultaneously. As Fig. 1(b) shown, we obtain two coherent elliptic Gaussian beams propagating along the z-axis by splitting light, which propagate on branch 1 and branch 2, respectively. The corresponding total energy flux density $\overline{\tilde{\mathbf{S}}}_{\mathrm{inf}}$

becomes the superposition of the individual elliptical Gaussian beam energy fluxes and their interaction, which could be

$$\overline{\tilde{\mathbf{S}}}_{\text{inf}} = \overline{\tilde{\mathbf{S}}}_1 + \overline{\tilde{\mathbf{S}}}_2 + \overline{\tilde{\mathbf{S}}}_{12} \tag{9}$$

where $\overline{\tilde{\mathbf{S}}}_{12}$ reflects the interference effect originated from interaction between the EM in branch 1 and 2, which is

$$\overline{\tilde{\mathbf{S}}}_{12} = \frac{1}{2\mu_0} \langle \tilde{\mathbf{E}}_1 \times \tilde{\mathbf{B}}_2 + \tilde{\mathbf{E}}_2 \times \tilde{\mathbf{B}}_1 \rangle \tag{10}$$

Due to $\tilde{E}_{1z} = \tilde{E}_{2z} = 0$, and branch 2 has rotated vertically (*i.e.*, $\tilde{E}_{1x} = \tilde{E}_{2y} = \psi/2$)

$$\tilde{E}_{1y} \sim \frac{2x}{W_x^2} \int \psi \, dy \tag{11a}$$

$$\tilde{E}_{2x} \sim \frac{2x}{W_y^2} \int \psi \, dx \tag{11b}$$

Combining Eqs. (2) and (3), $\tilde{B}_{1y} = \tilde{B}_{2x}$. The components of total energy flux density $\overline{\tilde{\mathbf{S}}}_{\text{inf}}$ are

$$\overline{\tilde{S}}_{\text{inf}_x}(y, z)\Big|_{x = d}$$

$$= \frac{1}{2\mu_0} \left[\text{Re}(\tilde{E}_{2y}^* \tilde{B}_{2z}) + \text{Re}(\tilde{E}_{1y}^* \tilde{B}_{1z}) + \text{Re}(\tilde{E}_{2y}^* \tilde{B}_{1z}) + \text{Re}(\tilde{E}_{1y}^* \tilde{B}_{2z}) \right]\Big|_{x = d} \tag{12}$$

$$\overline{\tilde{S}}_{\text{inf}_y}(x, z)\Big|_{y = d}$$

$$= \frac{1}{2\mu_0} \left[\text{Re}(\tilde{E}_{1x}^* \tilde{B}_{1z}) + \text{Re}(\tilde{E}_{2x}^* \tilde{B}_{2z}) + \text{Re}(\tilde{E}_{1x}^* \tilde{B}_{2z}) + \text{Re}(\tilde{E}_{2x}^* \tilde{B}_{1z}) \right]\Big|_{y = d} \tag{13}$$

$$\overline{\tilde{S}}_{\text{inf}_x}(x, y)\Big|_{z = d}$$

$$= \frac{1}{2\mu_0} \left[\text{Re}(\tilde{E}_{1x}^* \tilde{B}_{1y} - \tilde{E}_{1y}^* \tilde{B}_{1x}) + \text{Re}(\tilde{E}_{2x}^* \tilde{B}_{2y} - \tilde{E}_{2y}^* \tilde{B}_{2x}) \right.$$

$$\left. + \text{Re}(\tilde{E}_{1x}^* \tilde{B}_{2y} - \tilde{E}_{1y}^* \tilde{B}_{2x}) + \text{Re}(\tilde{E}_{2x}^* \tilde{B}_{1y} - \tilde{E}_{2y}^* \tilde{B}_{1x}) \right]\Big|_{z = d} \tag{14}$$

It should be noted that when $W_{0x}/W_{0y} = W_{0y}/W_{0x}$, $\overline{\tilde{S}}_{\text{inf}_x}(y, z)\Big|_{x = d} = \overline{\tilde{S}}_{\text{inf}_y}(x, z)\Big|_{y = d}$. As a result, $I_{\text{inf}}(x) = I_{\text{inf}}(y)$ after interference.

The simulated results of interference between two coherent elliptical Gaussian beams are illuminated in Figs. 4–6, which show: 1) As above theoretical derivations Eqs. (11)–(13), when $W_{0x}/W_{0y} = W_{0y}/W_{0x}$, the energy flux on x axis is equivalent with the result on y direction; 2) With the increase of W_{0x}/W_{0y}, the transverse intensity increases after interference. Therefore in the following simulation, we choose W_{0x}/W_{0y}
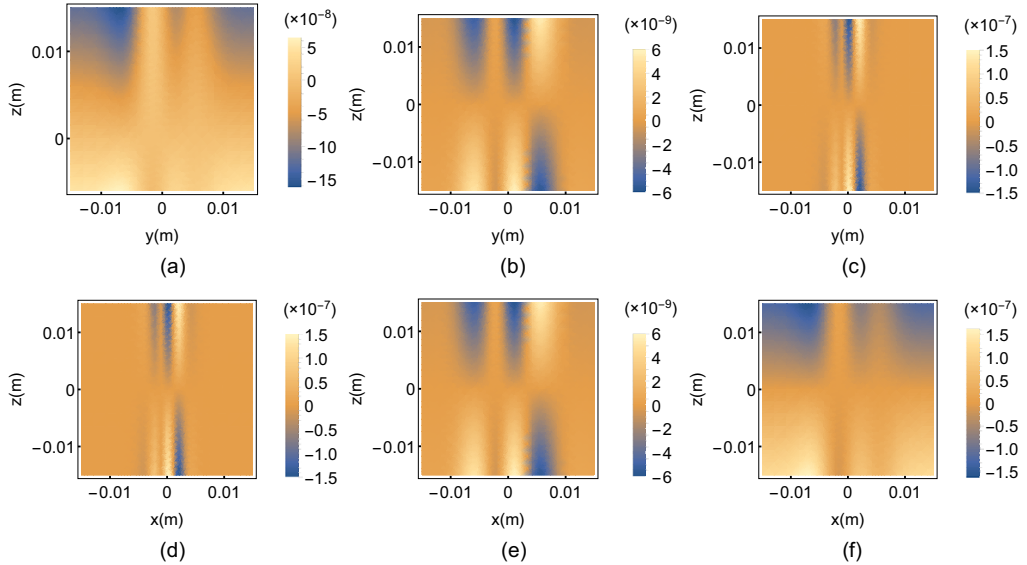

Fig. 4. The transverse energy flux density $\overline{S}_{\inf_x}(y, z)\big|_{x=d}$, $\overline{S}_{\inf_y}(x, z)\big|_{y=d}$ of two coherent beams after interference. The first column subplots (a) and (d) represent $\overline{S}_{\inf_x}(y, z)\big|_{x=d}$ and $\overline{S}_{\inf_y}(x, z)\big|_{y=d}$, respectively, with $W_{0x} = 0.002$ m, $W_{0y} = 0.005$ m; The second column subplots (b) and (e) represent $\overline{S}_{\inf_x}(y, z)\big|_{x=d}$ and $\overline{S}_{\inf_y}(x, z)\big|_{y=d}$, respectively, with $W_{0x} = W_{0y} = 0.005$ m; The third column subplots (c) and (f) represent $\overline{S}_{\inf_x}(y, z)\big|_{x=d}$ and $\overline{S}_{\inf_y}(x, z)\big|_{y=d}$, respectively, with $W_{0x} = 0.005$ m, $W_{0y} = 0.002$ m.
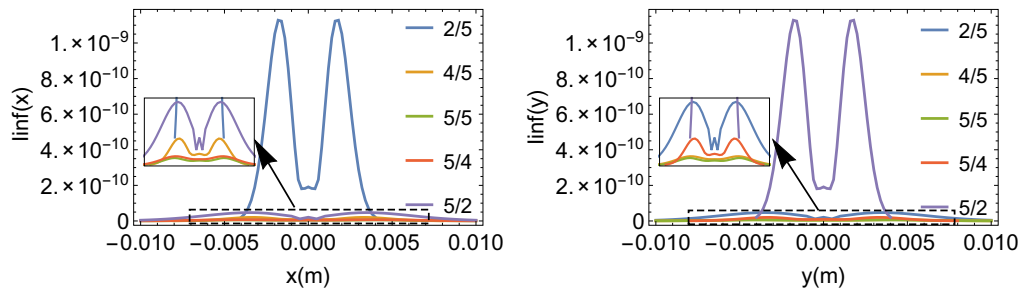

Fig. 5. The transverse intensity distribution of two beams after interference. The values on the legend represent the values of W_{0x}/W_{0y}. Here 2/5 represents $W_{0x} = 0.002$ m, $W_{0y} = 0.005$ m, while 5/2 represents $W_{0x} = 0.005$ m, $W_{0y} = 0.002$ m; 4/5 represents $W_{0x} = 0.004$ m, $W_{0y} = 0.005$m, while 5/4 represents $W_{0x} = 0.005$ m, $W_{0y} = 0.004$ m; 5/5 represents $W_{0x} = W_{0y} = 0.005$ m.
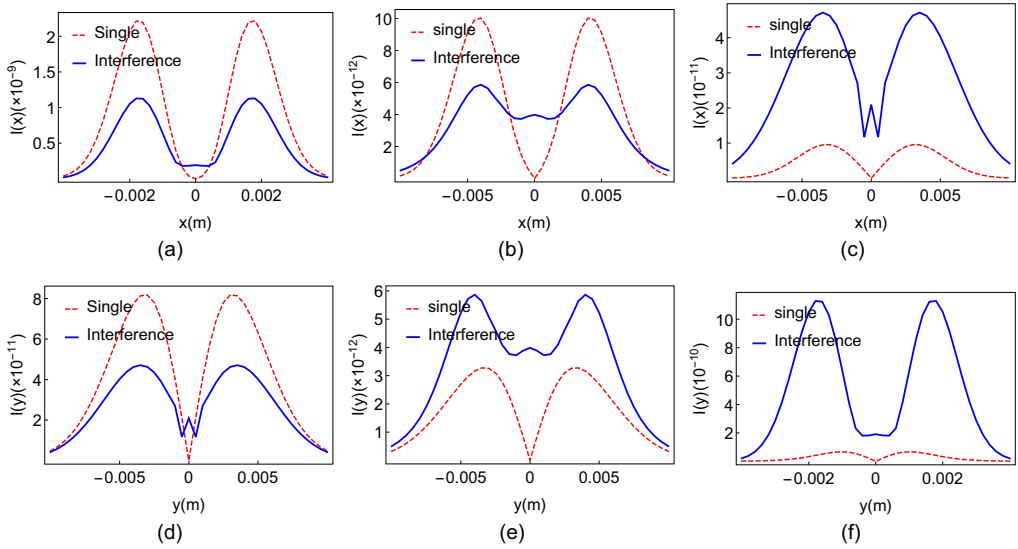
Fig. 6. The comparison of transverse intensity distributions before and after interference with different waist ratios. In the first column subplots (a) and (d), $W_{0x} = 0.002$ m and $W_{0y} = 0.005$ m. In the second column subplots (b) and (e), $W_{0x} = W_{0y} = 0.005$ m. In the third column subplots (c) and (f), $W_{0x} = 0.005$ m and $W_{0y} = 0.002$ m.

$= 5/2$. It is worth noting that we do not further increase the value of W_{0x}/W_{0y} here, because with the beam quality guaranteed, *i.e.*, the M^2 factor should be not too low, the eccentricity of the light spot should be kept between 0 and 0.5 as possible [24].

From above results, it is found that using the EGB with larger eccentricity is helpful to enhance the local transverse intensity after interference. More generally, the EGB_2 can be replaced by other electromagnetic (EM) field with the similar polarization. That provides a possible approach to improve transverse weak signal detection.

4. Detectability

Due to the weakness of the transverse energy flux, the detectability is influenced by noise significantly. Then we mainly discuss the shot noise and the noise caused by incomplete extinction of the longitudinal electric field $\tilde{E}_z$. (Note: in our case, the noise from Rayleigh scattering (RS), which has the intensity ratio to incident intensity as $I_{RS}/I_0 \sim (2\pi/\lambda)^4(l/2)^6$ (l is the size of scattering particle setting as $\lambda/10$), is much weaker than the signal, so it is not concerned in the following content.)

The energy flux density of shot noise, which is generated from quantum fluctuations of photons, can be calculated by [17]

$$\overline{\tilde{S}}_{\text{shot}} = \hbar v \sqrt{N_x} \tag{15}$$

where v is the frequency of EGB, N_x is the sum of the number of background transverse photon flux and transverse signal photon flux. According to the above experiment
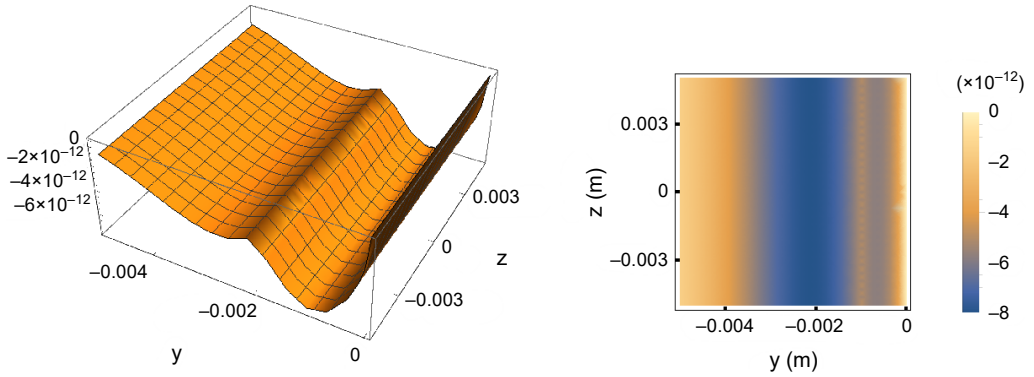
Fig. 7. The 3D and 2D graphs of shot noise energy flux density $(\text{J}\cdot\text{s}^{-1}\cdot\text{m}^{-2})$ on yz plane at $x = 0.01$ m.

parameters and fixing $W_{0x} = 5$ mm, $W_{0y} = 2$ mm, the detector located at $d = 1$ cm, the energy flux density of shot noise behaves as Fig. 7.

In the above theoretical derivations, the longitudinal electrical component of the Gaussian beam $\tilde{E}_z = 0$, but in the actual experiment, $\tilde{E}_z$ is not strictly zero due to the inevitable longitudinal EM components at the propagation position away from the waist. So when $\tilde{E}_z \neq 0$ (here we suppose that the amplitude of the longitudinal electrical component is about $1/10^4$ of the amplitude of the EGB), the electromagnetic components of EGB are derived as

$$\tilde{E}_x = \psi \tag{16a}$$

$$\tilde{E}_y = -\int \left(\frac{\partial \tilde{E}_x}{\partial x} + \frac{\partial \tilde{E}_z}{\partial z} \right) dy \tag{16b}$$

$$\tilde{E}_z = \psi / 10^4 \tag{16c}$$

$$\tilde{B}_x = \frac{i}{\omega} \left(\frac{\partial \tilde{E}_y}{\partial z} - \frac{\partial \tilde{E}_z}{\partial y} \right) \tag{17a}$$

$$\tilde{B}_y = \frac{i}{\omega} \left(\frac{\partial \tilde{E}_z}{\partial x} - \frac{\partial \tilde{E}_x}{\partial z} \right) \tag{17b}$$

$$\tilde{B}_z = \frac{i}{\omega} \left(\frac{\partial \tilde{E}_x}{\partial y} - \frac{\partial \tilde{E}_y}{\partial x} \right) \tag{17c}$$

Therefore the corresponding energy flux density of noise from incomplete extinction on x-axis $P_{\tilde{E}_z}$ can be calculated by

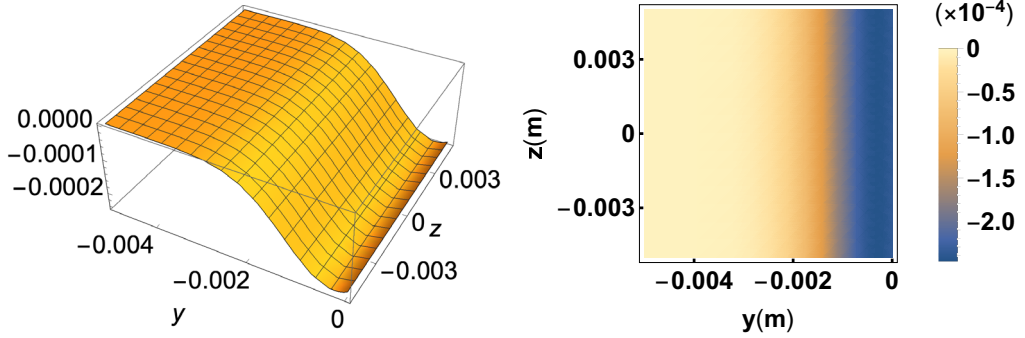$$\overline{\tilde{S}_{\tilde{E}_z}} = \frac{1}{2\mu_0} \text{Re}(\tilde{E}_y^* \tilde{B}_z - \tilde{E}_z^* \tilde{B}_y) \tag{18}$$

Fig. 8. The 3D and 2D graphs of noise energy flux density $(J \cdot s^{-1} \cdot m^{-2})$ caused by incomplete $\tilde{E}_z$ extinction at $x = 0.01$ m. Here $W_{0x} = 0.005$ m, $W_{0y} = 0.002$ m.

Figure 8 shows the spatial distribution of $\overline{\tilde{S}}_{\tilde{E}_z}$.

Combining the above energy flux density of signal (*i.e.*, Eq. (12)) and noises, the optimal detection area can be found in Fig. 9, which is around $y = -2$ mm where the noise from incomplete extinction (NEz) is opposite to the propagation direction of the signal (PPF), furthermore the signal reaches the maximum value. Therefore the corresponding signal to noise ratio is $I_{\text{PPF}}/I_{\text{shot noise}} = 1.33 \times 10^7$, which is available to verify the detection of transverse photon flux in optical frequency band.
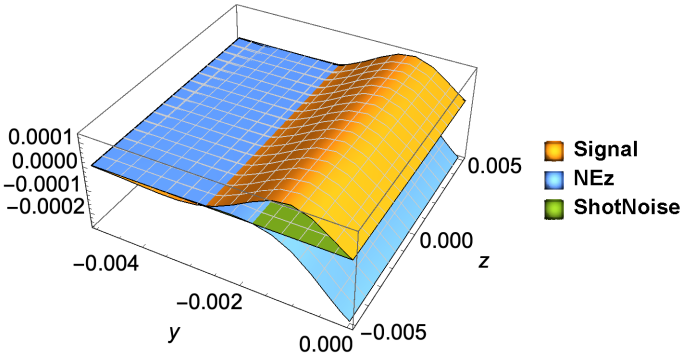

Fig. 9. The energy flux density comparison of signal.

5. Conclusion and remarks

In our results, the energy flux and intensity of a single EGB are not equivalent between *x*- and *y*-axes, which should be originated from the initial conditions of the electromagnetic components. In the interference process, due to the initial condition on *x*- and *y*-axes being exchanged on branch 2, the inference energy flux density and intensity along *x* and *y* directions behave similarly with the same eccentricity.

As a single EGB, its energy flux density on transverse plane is barely different from the CGB, but on longitudinal plane it reflects the geometric differences significantly. But the intensities in transverse directions are influenced by waist ratio greatly. Our results indicate that the intensity on transverse regions could become stronger with larger eccentricity of waist. In the phenomenon of interference, the advantage of using EGB to further strengthen the transverse energy is verified by numerical simulation. After calculating the energy density of shot noise and noise from incomplete extinction, it is found that in the *yz* plane with –2 mm < *y* < 0 the propagation of signal (*i.e.*, transverse photon flux) is opposite to the directions of the noises from incomplete extinction and the signal-to-noise ratio is enhanced significantly. Those results support an effective approach to raise transverse energy through adjusting waist ratio to a specific value with interference. Therefore the EGB has great potential for the research and experiment using transverse energy.

In the above mentioned extra-high gravitational wave detection, the optical branch 2 would be replaced by the EM field yielded by the interaction between gravitational wave and static magnetic field, and the laser frequency would be decreased into microwave band. However the EM response is similar with this work, so our results provide a pilot test in optic frequency band for such experiment.

References

[1] CAI Y., HE S., *Average intensity and spreading of an elliptical Gaussian beam propagating in a turbulent atmosphere*, Optics Letters **31**(5), 2006: 568-570. https://doi.org/10.1364/OL.31.000568

[2] SHEN J., LIU X., WANG W., YU H., *Calculation of light scattering of an elliptical Gaussian beam by a spherical particle*, Journal of the Optical Society of America A **35**(8), 2018: 1288-1298. https://doi.org/10.1364/JOSAA.35.001288

[3] ARNAUD J.A., KOGELNIK H., *Gaussian light beams with general astigmatism*, Applied Optics **8**(8), 1969: 1687-1693. https://doi.org/10.1364/AO.8.001687

[4] CARTER W.H., *Electromagnetic field of a Gaussian beam with an elliptical cross section*, Journal of the Optical Society of America **62**(10), 1972: 1195-1201. https://doi.org/10.1364/JOSA.62.001195

[5] DUAN K., LÜ B., *Propagation properties of vectorial elliptical Gaussian beams beyond the paraxial approximation*, Optics & Laser Technology **36**(6), 2004: 489-496. https://doi.org/10.1016/j.optlastec.2003.12.011

[6] SESHADRI S.R., *Basic elliptical Gaussian wave and beam in a uniaxial crystal*, Journal of the Optical Society of America A **20**(9), 2003: 1818-1826. https://doi.org/10.1364/JOSAA.20.001818

[7] GIULIANO C.R., DEBOIS D.F., HELLWARTH R.W., HESS L.D., RICKEL G.R., *Damage threshold studies in laser crystals*, Tech. Rep. (HUGHES RESEARCH LABS MALIBU CA, 1972).

[8] CORNOLTI F., LUCCHESI M., ZAMBON B., *Elliptic Gaussian beam self-focusing in nonlinear media*, Optics Communications **75**(2), 1990: 129-135. https://doi.org/10.1016/0030-4018(90)90241-K

[9] ALDA J., WANG S., BERNABEU E., *Analytical expression for the complex radius of curvature tensor Q for generalized Gaussian beams*, Optics Communications **80**(5-6), 1991: 350-352. https://doi.org/10.1016/0030-4018(91)90421-9

[10] Qiang L., Shaomin W., Alda J., Bernabeu E., *Transformation of nonsymmetric Gaussian-beam into symmetrical one by means of tensor ABCD law*, Optik **85**(2), 1990: 67-72.

[11] Medhekar S., Konar S., Sodha M.S., *Self-tapering of elliptic Gaussian beams in an elliptic-core nonlinear fiber*, Optics Letters **20**(21), 1995: 2192-2194. https://doi.org/10.1364/OL.20.002192

[12] Freegarde T., Coutts J., Walz J., Leibfried D., Hänsch T.W., *General analysis of type I second -harmonic generation with elliptical Gaussian beams*, Journal of the Optical Society of America B **14**(8), 1997: 2010-2016. https://doi.org/10.1364/JOSAB.14.002010

[13] Li F.-Y., Tang M.-X., Shi D.-P., *Electromagnetic response of a Gaussian beam to high-frequency relic gravitational waves in quintessential inflationary models*, Physical Review D **67**(10), 2003: 104008. https://doi.org/10.1103/PhysRevD.67.104008

[14] Li F., Baker R.M. Jr, Fang Z., Stephenson G.V., Chen Z., *Perturbative photon fluxes generated by high-frequency gravitational waves and their physical effects*, European Physical Journal C **56**(3), 2008: 407-423. https://doi.org/10.1140/epjc/s10052-008-0656-9

[15] Li F., Yang N., Fang Z., Baker R.M.L. Jr, Stephenson G.V., Wen H., *Signal photon flux and background noise in a coupling electromagnetic detecting system for high-frequency gravitational waves*, Physical Review D **80**(6), 2009: 064013. https://doi.org/10.1103/PhysRevD.80.064013

[16] Li F.-Y., Yang N., *Phase and polarization state of high-frequency relic gravitational waves*, Chinese Physics Letters **26**(5), 2009: 050402. https://doi.org/10.1088/0256-307X/26/5/050402

[17] Li J., Lin K., Li F., Zhong Y., *The signal photon flux, background photons and shot noise in electromagnetic response of high-frequency relic gravitational waves*, General Relativity and Gravitation **43**(8), 2011: 2209-2222. https://doi.org/10.1007/s10714-011-1176-8

[18] Li Fang-Yu, Wen Hao, Fang Zhen-Yun, *High-frequency gravitational waves having large spectral densities and their electromagnetic response*, Chinese Physics B **22**(12), 2013: 120402. https://doi.org/10.1088/1674-1056/22/12/120402

[19] Wen H., Li F., Fang Z., *Electromagnetic response produced by interaction of high-frequency gravitational waves from braneworld with galactic-extragalactic magnetic fields*, Physical Review D **89**(10), 2014: 104025. https://doi.org/10.1103/PhysRevD.89.104025

[20] Zhong Y.-H., Li J., Zhou Y., Lei Q.-L., *Electromagnetic resonance of astigmatic Gaussian beam to the high frequency gravitational waves*, Chinese Physics Letters **33**(10), 2016: 100402. https://doi.org/10.1088/0256-307X/33/10/100402

[21] Zhong Y., Liu S., Yang P., *Energy flux of a Gaussian beam in microwave band beyond the paraxial approximation*, Optik **125**(22), 2014: 6657-6660. https://doi.org/10.1016/j.ijleo.2014.08.125

[22] Xiang F., Zhang L., Chen T., Zhong Y.-H., Li J., *Transverse propagation characteristics and coherent effect of Gaussian beams*, Chinese Physics Letters **37**(6), 2020: 064101. https://doi.org/10.1088/0256-307X/37/6/064101

[23] Zhang X., Laser Technology **13**, 1989: 55.

[24] Liu X.L., Feng G.Y., Li W., Tang C., Zhou S.H., *Theoretical and experimental study on M-2 factor matrix for astigmatic elliptical Gaussian beam*, Acta Physica Sinica **62**(19), 2013: 194202. https://doi.org/10.7498/aps.62.194202